

# Does deep machine vision have just noticeable difference (JND)?

Jian Jin, *Member, IEEE*, Xingxing Zhang, Xin Fu, Huan Zhang, Weisi Lin, *Fellow, IEEE*, Jian Lou, Yao Zhao, *Senior Member, IEEE*,

**Abstract**—As an important perceptual characteristic of the Human Visual System (HVS), the Just Noticeable Difference (JND) has been studied for decades with image/video processing (e.g., perceptual image/video coding). However, there is little exploration on the existence of JND for AI, like Deep Machine Vision (DMV), although the DMV has made great strides in many machine vision tasks. In this paper, we take an initial attempt, and demonstrate that DMV does have the JND, termed as DMV-JND. Besides, we propose a JND model for the classification task in DMV. It has been discovered that DMV can tolerate distorted images with average PSNR of only 9.56dB (the lower the better), by generating JND via unsupervised learning with our DMV-JND-NET. In particular, a semantic-guided redundancy assessment strategy is designed to constrain the magnitude and spatial distribution of the JND. Experimental results on classification tasks demonstrate that we successfully find and model the JND for deep machine vision. Meanwhile, our DMV-JND paves a possible direction for DMV oriented image/video compression, watermarking, quality assessment, deep neural network security, and so on.

## I. INTRODUCTION

The unique psychological and physiological mechanism of the Human Visual System (HVS) makes humans cannot perceive certain changes in images/videos due to their underlying spatial/temporal sensitivity and masking properties [1]. That is, images/videos have visual redundancy for the HVS. The HVS oriented Just Noticeable Difference (JND), termed as HVS-JND, aims to find the maximum visual threshold of each pixel that changes under this threshold can be tolerated by the HVS (i.e., the homogeneous property of JND). The homogeneous property makes HVS-JND widely used in many image/video processing, such as perceptual image/video coding [1], quality evaluation of experience of image/video streaming [2], watermarking [3], error resilience [4], super resolution [5], graphic rendering [6], and so on.

With massive data and high-performance GPU hardware, Deep Machine Vision (DMV) has made breakthroughs in many machine vision tasks. This big progress also makes the ultimate receiver and appreciator of image/video change from HVS to DMV. Many image/video processing applications are developed for DMV now, and we naturally wonder: does DMV have the JND? Unlike the HVS-JND aiming to find the visual redundancy for HVS, the JND for DMV is expected to be able to find the redundancy of the image/video for the deep machine vision (like deep CNNs) by considering the effects of such redundancy during DMV tasks. If DMV does have JND, the JND for DMV will greatly benefit the DMV oriented image/video applications. For instance, it would

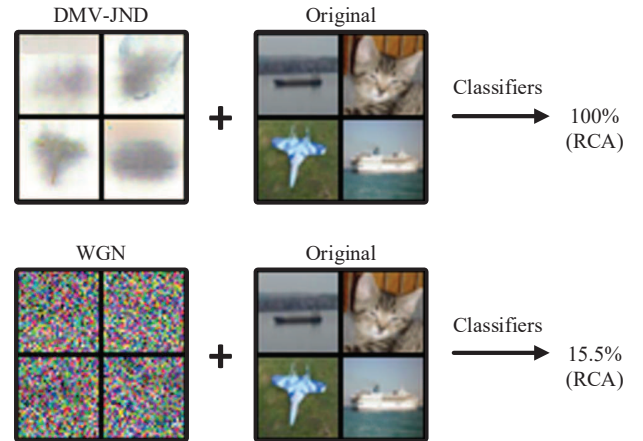


Fig. 1. The RCA comparison between DMV-JND-distorted image and random-noise-distorted image. After adding DMV-JND (generated via our proposed DMV-JND model) and WQN to the original image, we get 100% and 15.55% RCA on the CIFAR-10 dataset, respectively.

help to design novel codecs for AI-oriented image/video compression [7] via an DMV-JND inspired accurate bit rate allocation strategy, e.g., less/more bit rate is assigned to the region with more/less redundancy for DMV to achieve overall bit rate saving within the tolerance of the DMV. Besides, it may provide us a novel perspective for a wider scope, e.g., DMV oriented image/video quality evaluation, for natural images/videos, computer-generated images/videos [8], style transformation images/videos [9], and even for rethinking of the deep neural network security (e.g., adversarial sample generation [10] and attack [11]).

In this paper, we make an initial exploration on the JND for DMV and propose the first model to demonstrate the existence of DMV oriented JND, termed as DMV-JND. As shown in Fig. 1, our generated DMV-JND can be tolerated by the classification task, while the same level random noise (White Gaussian Noise, WQN) is noticed by the DMV and leads to significantly lower **Relative Classification Accuracy (RCA)**. RCA is calculated with classifier-generated labels (generated by inputting the original image into four commonly used classifiers, as to be discussed in Subsection III-A) instead of their corresponding handcrafted one. The reason for using classifier-generated labels instead of the handcrafted one is to be elaborated in Subsection III-A.

The main contributions in this research are summarized as follows.

- To the best of our knowledge, our work is the first to demonstrate that DMV does have the JND. Besides, we also propose the first algorithmic framework to model DMV-JND.
- The proposed DMV-JND model, achieved via unsupervised learning with our DMV-JND-NET, is capable of generating DMV-JND-distorted image with average PSNR of only 9.56dB for DMV.
- A semantic-guided redundancy assessment strategy is introduced to facilitate the reasonability of the generated DMV-JND, by restraining the magnitude and spatial distribution of the DMV-JND .
- Reducing the noise from DMV-JND to zero, DMV maintains the RCA throughout the process; This demonstrates that DMV has the same homogeneous property as the HVS-JND.

## II. RELATED WORK

### A. HVS-JND

There has been substantial research in HVS-JND (i.e., the maximum change in the visual content can be tolerated by the most of human subjects) during the past decades [1], [12]–[20]. Commonly, The HVS can tolerate distorted images with average PSNR from 25 to 35 dB for the existing HVS-JND models [12]–[14], [18], which can be divided into two categories: i) pixel-domain-HVS-JND models can directly obtain the HVS-JND threshold of each pixel by leveraging the background luminance, and various textural masking effects [12]–[14]; ii) sub-band-domain-HVS-JND models usually transfer the pixel domain image to the sub-band domain via discrete cosine transformation (or another transformation) first, and then the HVS-JND threshold on sub-band domain is estimated by taking the contrast sensitive function, luminance adaptation [16], and the contrast masking [15] and other textural masking effects into account. However, the HVS-JND threshold for each pixel/sub-band is often separately estimated in pixel/sub-band domain and summed up in a local neighborhood, and cannot represent the total masking of the whole image. Some recent works [17], [19], [20] propose learning-based HVS-JND models using databases with subjective HVS-JND tests conducted at whole picture/video level, for image/video coding situations.

All the techniques and advantages of HVS-JND above can only be applied to the applications in which HVS is the ultimate receiver and appreciator. For DMV applications, JND for DMV should be restudied and redesigned.

### B. Perceptual Image/Video Coding

As HVS-JND can predict the visual redundancy of images/videos, and this makes it widely used in perceptual images/videos coding. HVS-JND can be used to design filters [21] to reduce the redundancy information, bringing about bit rate saving when the filtered image is compressed. Besides, HVS-JND can also be used to guide the bit rate allocation [22], [23] during rate distortion optimization, and for speeding up the motion estimation process [13].

### C. Class Activation Mapping (CAM)

CAM is firstly proposed by Zhou *et al.* [24]. They find that revisiting the global average pooling layer for classification can actually build a localizable representation to expose the implicit attention of CNNs on an image. By utilizing this technique, the importance of different regions in the image, which leads to the image being classified to the specified class, can be represented with a CAM image. As shown in Fig. 2, when original image (a) and (c) are classified to “car”, the important region corresponding to “car” will be highlighted in their associated CAM images (b) and (d). The value of a pixel in CAM image is from 0 to 1. The brightness of the pixel indicates the importance of pixel for the specified class with classification tasks. Given the specified class, this technique locates its corresponding object in the image. Hence, it is widely used in many weakly supervised object localization works [25]–[28].

### D. Adversarial Attack

As deep neural networks (DNNs) have achieved great successes in many applications, their security has attracted more attention in these years. Adversarial samples [10] are crafted by various adversarial attack [11] methods to fool the DNNs, which are expected to have the similar appearances with the clean ones, while can produce high confidence incorrect predictions. Generally, adversarial attacks can be divided into two categories, i.e., white-box attacks [11], [29] and black-box attacks [30]–[35]. White-box attacks are easier to fool the DNNs due to having their complete information, e.g., the structure and the parameters of the victim DNNs, which can find the more effective attacks way. For the generalized application scenes, the complete information of vast DNNs are hardly obtained before attacks. Black-box attacks are more applicable to vast DNNs need to attack their common vulnerability. The ultimate goal is to build more robust DNNs based on the vulnerabilities, which are expected to be able to effectively defense more kinds of attacks.

## III. PROBLEM DESCRIPTION AND FORMULATION

### A. Problem Description

HVS-JND models aim to find the visual redundancy of images/videos, by finding the HVS-JND (threshold) of each pixel (or the associated sub-bands), as already introduced in Subsection II-A. Any changes on each pixel under its associated HVS-JND cannot be perceived by the HVS. A benchmark of HVS-JND modeling assessment is the magnitude of the tolerated HVS-JND: without being perceived by the HVS, the higher HVS-JND is tolerated, the better HVS-JND models is. Similarly, the DMV-JND model is defined in this paper with reference to the HVS-JND model. Unlike human eyes being the final receptor of HVS-JND, our proposed DMV-JND model is DMV task oriented. Therefore, our proposed DMV-JND model is to find the visual redundancy characteristic of the images/videos for DMV tasks, for each pixel. Any changes under the DMV-JND magnitude will not affect the

performance of DMV tasks. We select the image classification as the DMV task in this paper, and the extension to other types of DMV tasks are expected and will be demonstrated in the future work.

As mentioned above, HVS-JND models are built for the human eyes. The difference between the HVS-JND-distorted image and the original one is commonly assessed by the human subjects as the ground truth during building HVS-JND data set [17], [19]. In this paper, the classifier-generated labels generated with four commonly used classifiers (AlexNet [36], VGG [37], ResNet [38], and DenseNet [39]) are chosen as our ground truth labels, since the final receptors in our model are DMV tasks (classifiers). Each of these classifiers can be regarded as a successful artificial machine vision system due to their high performance. Although they may have small differences, the main techniques (convolution, pooling, randomly dropout and so on) that they used are the same, which suggests that they may have similar DMV-JND characteristic. Therefore, selecting classifier-generated labels as ground truth instead of the handcrafted one (generated by human eyes) is more reasonable and generalizable for our DMV-JND modeling.

## B. Formulation

Assume  $C_n(\cdot)$  is the  $n^{\text{th}}$  classifier among these four classifiers, where  $n = 1, 2, 3, 4$ .  $x$  denotes the original image. Its associated DMV-JND image and the DMV-JND-distorted image are  $e$  and  $\hat{x}$ , respectively;  $\hat{x} = x + e$ . Therefore, the classifier-generated labels (regarded as ground truth labels) and their associated distorted ones, generated by feeding  $x$  and  $\hat{x}$  to the  $n^{\text{th}}$  classifier, can be denoted by  $C_n(x)$  and  $C_n(x+e)$ . Then, the DMV-JND modeling can be initially formulated as

$$\arg \min_e \left( \sum_n \text{cross-entropy}(C_n(x+e), C_n(x)) + \gamma \cdot \frac{1}{|e|} \right), \quad (1)$$

where  $\text{cross-entropy}(\cdot)$  denotes the cross-entropy loss. The first term in Eq. (1) ensures the distortion in the DMV-JND-distorted image can be tolerated by these four classifiers. The second term requires the DMV-JND  $e$  as large as possible.  $\gamma$  is a weight to balance these two items. Therefore, the DMV-JND modeling can be achieved by learning a reasonable DMV-JND image  $e$  in a network. To achieve this, we propose a DMV-JND-NET. As no handcrafted labels are used during training (four classifier-generated labels are used as the ground truth label), our proposed DMV-JND-NET can generate the DMV-JND with unsupervised learning. However, during our exploration, the constrain on DMV-JND generation above is still not sufficient, which cannot well control the DMV-JND generation, i.e., during training, the results of the generated DMV-JND are not regulated.

HVS-JND models commonly have a redundancy assessment strategy, which makes the HVS-JND model adaptively adjust the magnitude of whole HVS-JND and the spatial distribution of HVS-JND according to the content of image: insensitive regions tolerate more noise, given with larger thresholds, while smaller thresholds is assigned to the sensitive regions.

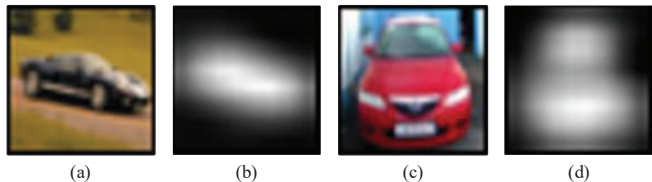


Fig. 2. Illustration of the important semantics. (a) and (c) are the original images. Their associated CAM images are (b) and (d).

To better control the DMV-JND generation, a similar redundancy assessment strategy is proposed in this paper, termed as semantic-guided redundancy assessment strategy. Since our target in this work is the classification with DMV, the sensitivity of DMV can be represented by the attention of classifier when the class is specified. As shown in Fig. 2 (a), there are car, trees, and ground. Assume that the class is specified “car”. DMV focuses on the pixels at car regions due to its high related semantic “car”. Although the pixels located at trees and ground contain some other semantics, they are ignored due to their unrelated semantics. Therefore, semantic-guided redundancy assessment strategy can be summarized as: pixel with high related semantic meaning has less redundancy, which tolerates less noise, assigned with smaller DMV-JND, while a larger DMV-JND is assigned to a pixel with larger redundancy due to its unrelated semantics. Since CAM image well reflects the semantic relevance of different pixels for classification tasks, it is used as a reference in our semantic-guided redundancy assessment strategy. Besides, our proposed assessment mechanism is further utilized to design two sub-losses (magnitude loss and spatial distribution loss), which constrain the magnitude and spatial distribution of the DMV-JND generation during training, respectively. More details will be elaborated in Section IV.

It should be noticed that our DMV-JND is quite different from adversarial attacks. First, different goals: the adversarial attacks are to find the most effective attack way (e.g., minimal noise) to change the final result (e.g., the label in the classification task). By contrast, DMV-JND tries to maintain the original result of the network by trying to maximum adding noise. Second, different applications: the adversarial attacks aim to find the vulnerability of current networks, thus further building a robust network. While our work is to find the redundancy for DMV for the basic DMV oriented image/video processing (e.g., compression or watermarking). Besides, our work is to find the DMV-JND threshold (boundary), any changes under this threshold will be tolerated by the DMV, namely any values under this threshold will not change the result of the networks, which are exhibited in Subsection V-F. However, the adversarial attack is more likely an optimal value, which may not guarantee that all the changes below it will make the network to achieve the same result.

## IV. DMV-JND-NET

### A. DMV-JND-NET: Architecture

The major components of the DMV-JND-NET include: three network parts (CAMs, E-D, Classifiers), and three opera-

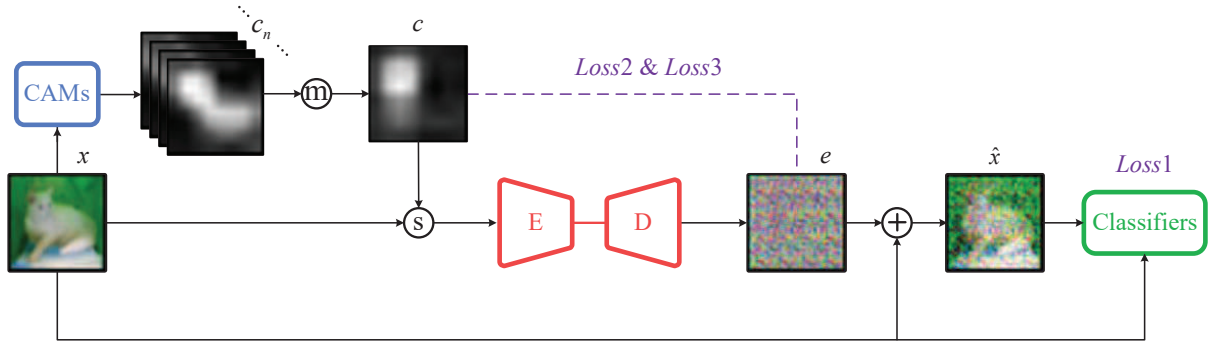


Fig. 3. The framework of the proposed DMV-JND-NET.

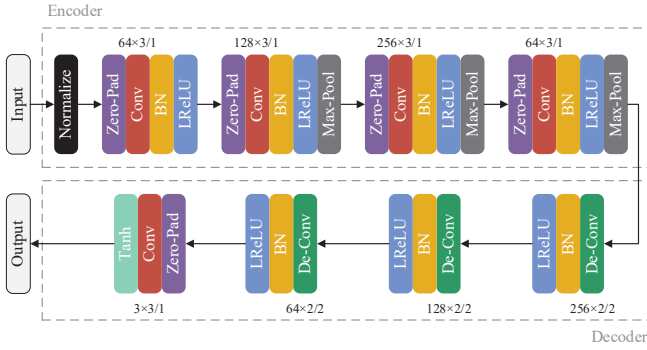


Fig. 4. Illustration of the hybrid convolutional autoencoder architecture used in this paper. The notation  $A \times B$  refers to  $B \times B$  convolutions with  $A$  filters. The number following the slash indicates stride in the case of convolutions. The zero padding and max pooling used here are set to  $(1, 1, 1, 1)$  and  $(2, 2)$ , respectively. BN is short for the batch normalization.

tions ( $\oplus$ ), ( $\otimes$ ), ( $\otimes$ ), as shown in Fig. 3.  $\otimes$  (merging operation) merges several images into one by applying a weighting calculation on corresponding pixels.  $\otimes$  (stacking operation) stacks several images together.  $\oplus$  (adding operation) adds one image to another by adding corresponding pixels. The details will be elaborated in Subsection IV-A.

CAMs are used to generate a merged CAM image. On the one hand, the merged CAM image is used to help to generate much richer features for DMV-JND generation. On the other hand, it is used as a reference during the semantical redundancy assessment of each input sample (original image). CAMs is made up of four CAM networks, which are revised from the aforementioned four classifiers (AlexNet, VGG, ResNet, and DenseNet) that appear as Classifiers in the figure. The revising and setting of CAMs in this paper refer to [24]. These four CAM networks have been pre-trained, and their weights are not updated during the DMV-JND-NET training.

E-D (hybrid convolutional autoencoder) is used to generate DMV-JND according to the content of each sample. It mainly contains a convolution plus pooling structure encoder and a large stride deconvolution structure decoder. A convolution plus pooling structure encoder is good at extracting robust features, which are widely used in image denoising [40]. A large stride deconvolution structure decoder can generate details, which is commonly used in image super-resolution

[41] and restoration [42]. With such a hybrid convolutional autoencoder, the semantic features can be robustly extracted at the encoder, and meanwhile, according to the extracted semantic features, more elaborated JND can be generated at the decoder side. Besides, padding, normalization operations are also used in our autoencoder. A more detailed structure of our autoencoder refers to Fig. 4. The parameters of this network are randomly initialized at first and then updated during training.

Classifiers are used to generate the classifier-generated labels and their associated distorted labels by feeding the original image and its associated DMV-JND-distorted image, which are further used to calculate a cross-entropy loss in our loss function. Similarly, all the classifiers are pre-trained, and their weights are not updated during the DMV-JND-NET training.

Assume the original image  $x$  is fed to the well trained CAMs at first. CAMs is made up of four CAM nets, denoted by  $C_1(\cdot)$ ,  $C_2(\cdot)$ ,  $C_3(\cdot)$  and  $C_4(\cdot)$ . Then, four CAM images are generated and denoted by  $c_1$ ,  $c_2$ ,  $c_3$  and  $c_4$ . For the  $n^{th}$  CAM image we have  $c_n = C_n(x)$ , where  $n = 1, 2, 3, 4$ . Then, the merging operation is applied to these four CAM images and a merged CAM image is generated, denoted by  $c$ . We have

$$c = \frac{1}{4} \sum_n c_n. \quad (2)$$

Then, the merged CAM image  $c$  together with the original image  $x$  are stacked via stacking operation and fed to the hybrid convolutional autoencoder  $E(\cdot)$  to generate DMV-JND image, denoted  $e$  under the loss function to be explored in the next subsection. We have

$$e = E(x, c). \quad (3)$$

After that, the generated DMV-JND image is added to the original image by applying adding operation on  $e$  and  $x$ , and we obtain the DMV-JND-distorted image  $\hat{x}$ , as we have already presented at the start of Subsection III-B:

$$\hat{x} = e + x. \quad (4)$$

Furthermore, the DMV-JND-distorted image  $\hat{x}$  and original image  $x$  are fed to Classifiers, which contains four corresponding classifiers, denoted by  $S_1(\cdot)$ ,  $S_2(\cdot)$ ,  $S_3(\cdot)$  and  $S_4(\cdot)$ . For

the  $n^{\text{th}}$  classifier, the distorted and true softmax values are denoted by  $\hat{\mathbf{s}}_n$  and  $\mathbf{s}_n$ , we have

$$\begin{cases} \hat{\mathbf{s}}_n = S_n(\hat{x}) \\ \mathbf{s}_n = S_n(x). \end{cases} \quad (5)$$

It should be noticed that  $\hat{\mathbf{s}}_n$  and  $\mathbf{s}_n$  are two vectors of probabilities of different labels. Assign the distorted and true labels by choosing the biggest elements in  $\hat{\mathbf{s}}_n$  and  $\mathbf{s}_n$ , and this process is represented by function  $M(\cdot)$ :

$$\begin{cases} \hat{l}_n = M(\hat{\mathbf{s}}_n) \\ l_n = M(\mathbf{s}_n), \end{cases} \quad (6)$$

where  $\hat{l}_n$  and  $l_n$  are the distorted label and classifier-generated label with the  $n^{\text{th}}$  classifier, respectively.

### B. DMV-JND-NET: Loss Functions

The overall loss function is made up of three sub-losses, namely cross-entropy loss, magnitude loss, and spatial distribution loss, denoted by  $Loss1$ ,  $Loss2$  and  $Loss3$ , respectively. They have different functionalities during directing the DMV-JND generation. Our overall loss is denoted by  $Loss$ , we have

$$Loss = Loss1 + \alpha \cdot Loss2 + \beta \cdot Loss3, \quad (7)$$

where  $\alpha$  and  $\beta$  are two weights to balance these three sub-losses, and set to 1 in this work.

The cross-entropy loss between the DMV-JND-distorted image  $\hat{x}$  and the original image  $x$  is to constrain the generated DMV-JND to make it tolerated by all these four classifiers during classification. For the  $n^{\text{th}}$  classifier, we have

$$Loss1_n = \text{cross-entropy}(\hat{\mathbf{s}}_n, l_n). \quad (8)$$

Therefore,  $Loss1$  can be represented as

$$Loss1 = \frac{1}{4} \sum_n Loss1_n. \quad (9)$$

For different images, the magnitudes of the redundant semantics are not the same, even though they may be specified with the same class label. As shown in Fig. 2, the dark region of (b) is larger than that of (d), and this means that there is more redundancy in (a) compared with (c). Our semantic-guided redundancy assessment strategy indicates that (a) is assigned with larger DMV-JND. To constrain the magnitude of DMV-JND according to the content of the original image  $x$ , magnitude loss is introduced. The average magnitude of the important semantics of each pixel in  $x$  is denoted by  $I$ , which can be defined as follows, based upon the merged CAM:

$$I = \frac{1}{HW} \sum_{h=1}^H \sum_{w=1}^W c(h, w). \quad (10)$$

$H$  and  $W$  are the height and width of the image  $x$ .  $c(h, w)$  ( $c(h, w) \in [0, 1]$ ) is the value of pixel  $(h, w)$  in the merged CAM image  $c$ . Therefore, the average magnitude of the redundancy of each pixel, namely the targeted average DMV-JND, denoted by  $N$ , can be defined as

$$N = 1 - I. \quad (11)$$

The actual average DMV-JND generated with our DMV-JND-NET is denoted by  $N_0$ , we have

$$N_0 = \frac{1}{HW} \sum_{h=1}^H \sum_{w=1}^W |e(h, w)|, \quad (12)$$

where  $|\cdot|$  is the operation of taking absolute value. Then,  $Loss2$  can be formulated as

$$\begin{aligned} Loss2 &= \ln \left( \frac{N^2 + N_0^2 + q}{2NN_0 + q} \right) \\ &= \ln(N^2 + N_0^2 + q) - \ln(2NN_0 + q). \end{aligned} \quad (13)$$

where  $q$  is a small constant to prevent the denominator from being zero, set to  $1^{-10}$ .

Initially,  $N$  is smaller than  $N_0$ .  $Loss2$  can make  $N$  approach to  $N_0$  during training. This makes sure that the actual average DMV-JND will be increasingly generated during training.

After the magnitude control of generated DMV-JND with magnitude loss above, the spatial distribution of DMV-JND should also be constrained according to the semantic-guided redundancy assessment strategy: a pixel with less redundancy is assigned with a smaller DMV-JND, while the one with more redundancy is assigned with a larger DMV-JND. To achieve this, the merged CAM image  $c$  is utilized again. Firstly, a vector  $\mathbf{v}$  is generated by applying softmax operation on  $c$ , and we have

$$\mathbf{v} = \text{softmax}(c). \quad (14)$$

Then, apply inner product  $\langle \cdot, \cdot \rangle$  between  $\mathbf{v}$  and  $e$ , and the spatial distribution loss can be formulated as

$$Loss3 = \langle \mathbf{v}, e \rangle. \quad (15)$$

$Loss3$  makes sure that higher DMV-JND is generated on the higher redundant pixels.

## V. EXPERIMENTS

### A. Dataset and Settings

We evaluate the proposed DMV-JND-NET on the CIFAR-10 dataset [43], which is widely used as the benchmark for image classification. The CIFAR-10 dataset consists of 60,000 32x32 color images in 10 classes, with 6,000 images per class, which are divided into 50,000 training images and 10,000 test images. All the classifiers used, including AlexNet, VGG, ResNet, and DenseNet, are pre-trained. The CAM nets used in this paper, such as AlexNet-CAM, VGG-CAM, ResNet-CAM, and DenseNet-CAM, are with the settings used in paper [24]. All the experiments are conducted on one NVIDIA GTX 1080 GPU with 8GB memory.

### B. RCA and Loss

The formulation of RCA is given in this subsection first. For the  $n^{\text{th}}$  classifier, its individual RCA is represented as

$$acc_n = \frac{100\%}{P} \sum^P \text{pre}(\hat{l}_n, l_n) \quad (16)$$

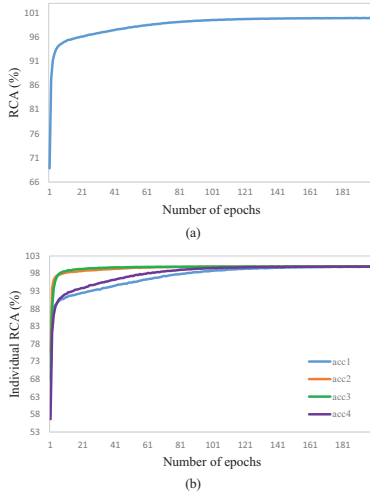


Fig. 5. Illustration of the training RCA trend, (a) is the RCA trend. Its associated individual RCA trend for each classifier is exhibited in (b).

$\sum \text{pre}(\cdot)$  is used to sum all the  $P$  prediction results, where the right/false result is represented as 1/0. Then, RCA is formulated by the average of four individual RCAs

$$\text{acc} = \frac{1}{4} \sum_n \text{acc}_n. \quad (17)$$

Fig. 5 (a) shows the trend of  $\text{acc}$ , which contains three stages: i) the fast process of RCA increasing stage is about from epoch 1 to epoch 10; ii) the slightly increasing stage is about from epoch 11 to epoch 140; and iii) the stable stage is about from epoch 141 to epoch 200 when the RCA reaches 100%. This result means that even DMV-JND is added via our DMV-JND model, the DMV-JND-distorted images still can be correctly classified by all these four classifiers. Besides, the individual RCA trend of each single classifier ( $\text{acc}_1, \dots, \text{acc}_4$ ) reaches 100% as well, as shown in Fig. 5 (b). It should be mentioned that all these results are for the training RCA. The testing RCA of the proposed DMV-JND-NET reaches 92.18%, and its associated individual RCA also reaches 91.17%, 93.03%, 93.48% and 91.05%, respectively. Although we cannot achieve a better testing RCA under achieving such magnitude DM-JND, this is enough to demonstrate that the our generated DMV-JND can be tolerated by four commonly used classifiers for classification. We believe this problem will be better solved in the following research.

Conversely, as epoch increases, the overall loss drastically reduces at first. Then, it is falling at a slower pace and finally converges to a value at 0.083, as shown in Fig. 6 (a). In addition, the trend of three  $\text{Loss}_1$ ,  $\text{Loss}_2$ , and  $\text{Loss}_3$  are also respectively shown in Fig. 6 (b), (c), and (d).  $\text{Loss}_1$  and  $\text{Loss}_2$  have typical falling trend. However, the trend of  $\text{Loss}_3$  is an increasing one. That is because as the training epoch increases,  $\text{Loss}_2$  decreases and  $N_0$  approaches  $N$ . Therefore, higher and higher DMV-JND is generated. This causes the increasing of  $e$  and then  $\text{Loss}_3$  increases. However,  $\text{Loss}_3$  still constrains the location of DMV-JND. This conclusion is further supported by the experimental results in Subsections V-C and V-D.

### C. Objective Results: PSNR

Fig. 7 shows the trend of the Peak Signal-to-Noise Ratio (PSNR) between the original image  $x$  and the DMV-JND-distorted image  $\hat{x}$ . As the epoch number increases, the PSNR firstly decreases dramatically. Then, the decreasing trend becomes a gradual process and eventually converges to 9.56 dB. The result is in line with our discussion in Subsection V-B: as the number of epoch increases, higher DMV-JND is generated with the decreasing of  $\text{Loss}_2$ , which leads to the increasing tendency of PSNR between the original image and the DMV-JND-distorted image; However, as the number of epoch increases, RCA increases as well, and this means that although higher DMV-JND is generated via our DMV-JND-NET, the generated DMV-JND's spatial distribution becomes more reasonable; That is because the generated DMV-JND is adjusted to more reasonable regions under the control of  $\text{Loss}_3$ ; The overall result is the decreasing PSNR trend in Fig. 7. In other words, the DMV-JND-NET is optimized towards a right direction. More visual evaluation results will be exhibited in the next subsection to support this point. It is worth to mention that DMV can tolerate the DMV-JND-distorted image with about 9.56 dB in our work, which is significantly smaller than the 25 to 35 dB in the HVS as mentioned in the Related Work above (Subsection II-A). This opens a new horizon for visual feature compression toward DMV. Of course, it needs to be understood that the HVS-JND is an absolute JND for situations where the difference is undetectable in a strict psychophysical sense, while the DMV-JND is a utility-oriented JND that merely does not affect the intended utility (classification in this work). More research is called for investigation for their difference [44].

### D. Visual Evaluation

Fig. 8 shows the CAM images, DMV-JND images, original images, and DMV-JND-distorted images, from the left to the right. Each column contains four results corresponding to epoch 1, 15, 45, and 145. The white regions in CAM images suggest the low redundancy regions for the DMV, while the dark regions suggest the high redundancy regions. In DMV-JND images, gray color with (125, 125, 125) values in RGB color space suggest no DMV-JND added in, while the other colors indicate different levels of DMV-JND. As the epoch number increases, the gray color regions in DMV-JND images become less, and this means higher DMV-JND is generated with the decreasing of  $\text{Loss}_2$ . Meanwhile, the spatial distribution of the gray regions in DMV-JND images are adjusted to those indicated by white regions in CAM images gradually, which demonstrates that  $\text{Loss}_3$  can well regulate the spatial distribution of the generated DMV-JND, although  $\text{Loss}_3$  increases due to more noise generated. Therefore, the DMV-JND can be well-constrained during DMV-JND generation. All these results indicate that our loss function is designed reasonably in modeling the DMV-JND.

### E. WGN Test

For comparison, we add the same-level WGN as DMV-JND to the original images and generate the WGN-distorted images.

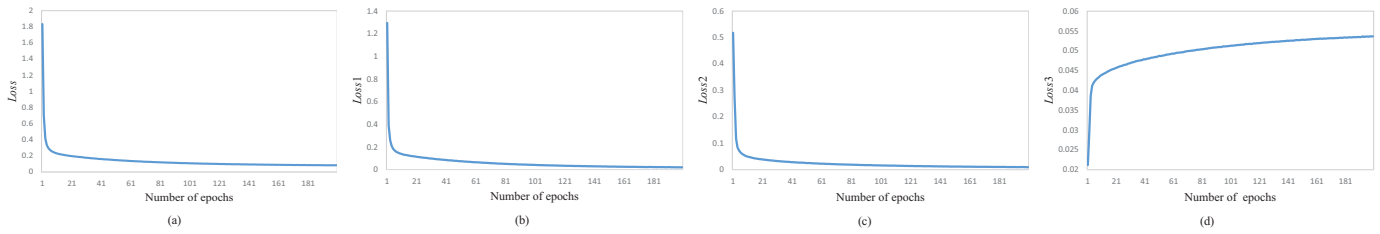


Fig. 6. Illustration of the training loss trend. (a) is the *Loss* in different epochs. Its associated *Loss1*, *Loss2*, and *Loss3* (notice the vertical scale difference) are exhibited in (b), (c) and (d), respectively.

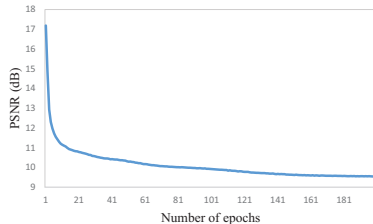


Fig. 7. Illustration of the PSNR trend.

These distorted images are fed to the classifiers, we get a much lower training RCA (i.e., 15.5%). In other words, adding random noise (WGN) leads to lower RCA, while adding the same-level DMV-JND via our DMV-JND-NET can achieve 100% training RCA as already shown in Fig. 1.

#### F. Homogeneous Property Test

As mentioned in Introduction, HVS-JND has the homogeneous property: the HVS cannot perceive the changes caused by reducing the added noise from the HVS-JND to zero. In this subsection, we verify that our proposed DMV-JND does have the similar homogeneous property: as the added noise is reduced from the DMV-JND to zero, the RCA of DMV is not changed.

To this end, we firstly get our trained DMV-JND-NET by fixing all the parameters of our DMV-JND model when the training RCA reaches 100%. Then, we generate 8 new below-DMV-JND images  $e_1, e_2, \dots, e_8$  for  $e$ , which has the  $8/9, 7/9, \dots, 1/9$  times of pixel value in  $e$ ; More specifically, assume the value of the  $k^{th}$  pixel in  $e$  is represented with  $v_k$ . Then, the  $k^{th}$  pixel value in  $e_1, e_2, \dots, e_8$  can be represented as  $v_{1,k} = \frac{8}{9}v_k, v_{2,k} = \frac{7}{9}v_k, \dots, v_{8,k} = \frac{1}{9}v_k$ . This process can be regarded as the noise reduction from our learned DMV-JND. For the CIFAR-10 dataset, there are 50,000 training images, with corresponding 50,000 DMV-JND images. Then, we feed 50,000 DMV-JND images,  $8 \times 50,000$  new below-JND images, and their associated 50,000 original images to our fixed classifiers and get the RCA being 100%. Therefore, our generated DMV-JND has the similar homogeneous property to that of the HVS-JND. All the noise below the DMV-JND can be tolerated by the DMV.

## VI. CONCLUSION

In this paper, we have demonstrated that the Deep Machine Vision (DMV) does has the just noticeable difference (JND),

termed as DMV-JND. We have built the first JND model for DMV. The problem formulation has been proposed for the DMV-JND, and the solution can be achieved by the proposed DMV-JND-NET by unsupervised learning. To better constrain DMV-JND generation, a semantic-guided redundancy assessment strategy is proposed and integrated into the DMV-JND-NET. Experimental results demonstrate that we successfully find and model the JND for AI vision (DMV). Thus, the proposed DMV-JND has great potential for deep machine vision oriented image processing.

## REFERENCES

- [1] N. Jayant, J. Johnston, and R. Safranek, "Signal compression based on models of human perception," *Proc. IEEE*, vol. 81, no. 10, pp. 1385–1422, 1993.
- [2] H. Zhang, H. Hu, G. Gao, Y. Wen, and K. Guan, "Deepqoe: A unified framework for learning to predict video qoe," in *IEEE Int. Conf. Multimedia and Expo*, 2018, pp. 1–6.
- [3] C.-H. Chou and K.-C. Liu, "A perceptually tuned watermarking scheme for color images," *IEEE Trans. Image Process.*, vol. 19, no. 11, pp. 2966–2982, 2010.
- [4] L. J. Karam and T.-T. Lam, "Selective error detection for error-resilient wavelet-based image coding," *IEEE Trans. Image Process.*, vol. 16, no. 12, pp. 2936–2942, 2007.
- [5] L. J. Karam, N. G. Sadaka, R. Ferzli, and Z. A. Ivanovski, "An efficient selective perceptual-based super-resolution estimator," *IEEE Trans. Image Process.*, vol. 20, no. 12, pp. 3470–3482, 2011.
- [6] G. Nader, K. Wang, F. Hétoy-Wheeler, and F. Dupont, "Just noticeable distortion profile for flat-shaded 3d mesh surfaces," *IEEE Trans. Vis. Comput. Graph.*, vol. 22, no. 11, pp. 2423–2436, 2015.
- [7] Z. Chen, K. Fan, S. Wang, L. Duan, W. Lin, and A. C. Kot, "Toward intelligent sensing: Intermediate deep feature compression," *IEEE Trans. Image Process.*, vol. 29, pp. 2230–2243, 2019.
- [8] T.-C. Wang, M.-Y. Liu, J.-Y. Zhu, G. Liu, A. Tao, J. Kautz, and B. Catanzaro, "Video-to-video synthesis," *arXiv preprint arXiv:1808.06601*, 2018.
- [9] Z. Yi, H. Zhang, P. Tan, and M. Gong, "Dualgan: Unsupervised dual learning for image-to-image translation," in *Int. Conf. Comput. Vis.*, 2017, pp. 2849–2857.
- [10] I. J. Goodfellow, J. Shlens, and C. Szegedy, "Explaining and harnessing adversarial examples," *arXiv preprint arXiv:1412.6572*, 2014.
- [11] S.-M. Moosavi-Dezfooli, A. Fawzi, and P. Frossard, "Deepfool: a simple and accurate method to fool deep neural networks," in *IEEE Conf. Comput. Vis. Pattern Recog.*, 2016, pp. 2574–2582.
- [12] C.-H. Chou and Y.-C. Li, "A perceptually tuned subband image coder based on the measure of just-noticeable-distortion profile," *IEEE Trans. Circuit Syst. Video Technol.*, vol. 5, no. 6, pp. 467–476, 1995.
- [13] X. Yang, W. Ling, Z. Lu, E. P. Ong, and S. Yao, "Just noticeable distortion model and its applications in video coding," *Signal Process. Image Commun.*, vol. 20, no. 7, pp. 662–680, 2005.
- [14] A. Liu, W. Lin, M. Paul, C. Deng, and F. Zhang, "Just noticeable difference for images with decomposition model for separating edge and textured regions," *IEEE Trans. Circuit Syst. Video Technol.*, vol. 20, no. 11, pp. 1648–1652, 2010.
- [15] Z. Wei and K. N. Ngan, "Spatio-temporal just noticeable distortion profile for grey scale image/video in dct domain," *IEEE Trans. Circuit Syst. Video Technol.*, vol. 19, no. 3, pp. 337–346, 2009.

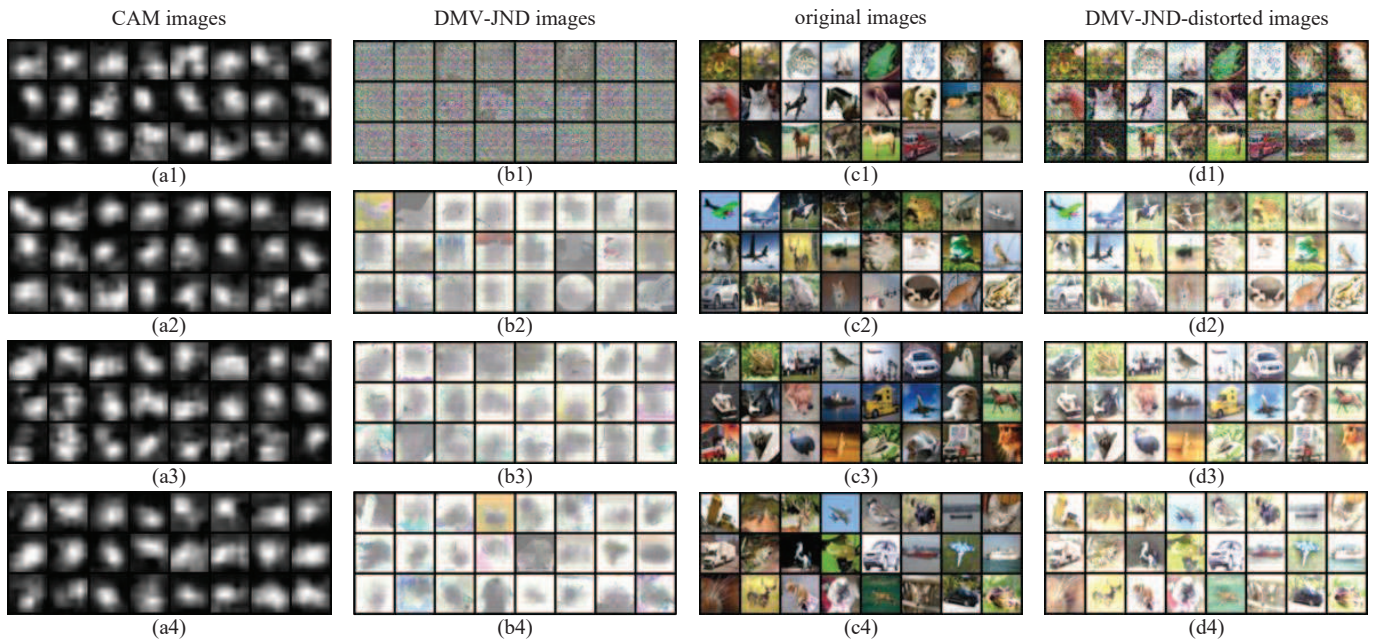


Fig. 8. (a1)–(a4) are the CAM images in epoch 1, 15, 45, and 145. Similarly, (b1)–(b4), (c1)–(c4), and (d1)–(d4) are the generated DMV-JND images, original images, and the DMV-JND-distorted images in epoch 1, 15, 45, and 145.

- [16] S.-H. Bae and M. Kim, “A novel dct-based jnd model for luminance adaptation effect in dct frequency,” *IEEE Sign. Process. Letters*, vol. 20, no. 9, pp. 893–896, 2013.
- [17] L. Jin, J. Y. Lin, S. Hu, H. Wang, P. Wang, I. Katsavounidis, A. Aaron, and C.-C. J. Kuo, “Statistical study on perceived jpeg image quality via mcl-ici dataset construction and analysis,” *Electronic Imaging*, vol. 2016, no. 13, pp. 1–9, 2016.
- [18] J. Wu, L. Li, W. Dong, G. Shi, W. Lin, and C.-C. J. Kuo, “Enhanced just noticeable difference model for images with pattern complexity,” *IEEE Trans. Image Process.*, vol. 26, no. 6, pp. 2682–2693, 2017.
- [19] H. Wang, I. Katsavounidis, J. Zhou, J. Park, S. Lei, X. Zhou, M.-O. Pun, X. Jin, R. Wang, X. Wang *et al.*, “Videoset: A large-scale compressed video quality dataset based on jnd measurement,” *J. Vis. Commun. Image Represent.*, vol. 46, pp. 292–302, 2017.
- [20] H. Liu, Y. Zhang, H. Zhang, C. Fan, S. Kwong, C.-C. J. Kuo, and X. Fan, “Deep learning-based picture-wise just noticeable distortion prediction model for image compression,” *IEEE Trans. Image Process.*, vol. 29, pp. 641–656, 2019.
- [21] J. Kim, S.-H. Bae, and M. Kim, “An hevc-compliant perceptual video coding scheme based on jnd models for variable block-sized transform kernels,” *IEEE Trans. Circuit Syst. Video Technol.*, vol. 25, no. 11, pp. 1786–1800, 2015.
- [22] Z. Luo, L. Song, S. Zheng, and N. Ling, “H. 264/advanced video control perceptual optimization coding based on jnd-directed coefficient suppression,” *IEEE Trans. Circuit Syst. Video Technol.*, vol. 23, no. 6, pp. 935–948, 2013.
- [23] M. Zhou, X. Wei, S. Kwong, W. Jia, and B. Fang, “Just noticeable distortion-based perceptual rate control in hevc,” *IEEE Trans. Image Process.*, vol. 29, pp. 7603–7614, 2020.
- [24] B. Zhou, A. Khosla, A. Lapedriza, A. Oliva, and A. Torralba, “Learning deep features for discriminative localization,” in *IEEE Conf. Comput. Vis. Pattern Recog.*, 2016, pp. 2921–2929.
- [25] J. Zhang, S. A. Bargal, Z. Lin, J. Brandt, X. Shen, and S. Sclaroff, “Top-down neural attention by excitation backprop,” *Int. J. Comput. Vis.*, vol. 126, no. 10, pp. 1084–1102, 2018.
- [26] Y. Wei, J. Feng, X. Liang, M.-M. Cheng, Y. Zhao, and S. Yan, “Object region mining with adversarial erasing: A simple classification to semantic segmentation approach,” in *IEEE Conf. Comput. Vis. Pattern Recog.*, 2017, pp. 1568–1576.
- [27] X. Zhang, Y. Wei, G. Kang, Y. Yang, and T. Huang, “Self-produced guidance for weakly-supervised object localization,” in *Eur. Conf. Comput. Vis.*, 2018, pp. 597–613.
- [28] X. Zhang, Y. Wei, J. Feng, Y. Yang, and T. S. Huang, “Adversarial complementary learning for weakly supervised object localization,” in *IEEE Conf. Comput. Vis. Pattern Recog.*, 2018, pp. 1325–1334.
- [29] A. Kurakin, I. Goodfellow, and S. Bengio, “Adversarial machine learning at scale,” *arXiv preprint arXiv:1611.01236*, 2016.
- [30] S. Cheng, Y. Dong, T. Pang, H. Su, and J. Zhu, “Improving black-box adversarial attacks with a transfer-based prior,” *arXiv preprint arXiv:1906.06919*, 2019.
- [31] A. Ilyas, L. Engstrom, and A. Madry, “Prior convictions: Black-box attacks with bandits and priors,” *arXiv preprint arXiv:1807.07978*, 2018.
- [32] Z. Yan, Y. Guo, and C. Zhang, “Subspace attack: Exploiting promising subspaces for query-efficient black-box attacks,” *arXiv preprint arXiv:1906.04392*, 2019.
- [33] N. Papernot, P. McDaniel, I. Goodfellow, S. Jha, Z. B. Celik, and A. Swami, “Practical black-box attacks against machine learning,” in *Proceedings of the 2017 ACM conference on computer and communications security*, 2017, pp. 506–519.
- [34] S.-M. Moosavi-Dezfooli, A. Fawzi, O. Fawzi, and P. Frossard, “Universal adversarial perturbations,” 2017, pp. 1765–1773.
- [35] Y. Dong, T. Pang, H. Su, and J. Zhu, “Evading defenses to transferable adversarial examples by translation-invariant attacks,” 2019, pp. 4312–4321.
- [36] A. Krizhevsky, I. Sutskever, and G. E. Hinton, “Imagenet classification with deep convolutional neural networks,” in *Adv. Neural Inform. Process. Syst.*, 2012, pp. 1097–1105.
- [37] K. Simonyan and A. Zisserman, “Very deep convolutional networks for large-scale image recognition,” *arXiv preprint arXiv:1409.1556*, 2014.
- [38] K. He, X. Zhang, S. Ren, and J. Sun, “Deep residual learning for image recognition,” in *IEEE Conf. Comput. Vis. Pattern Recog.*, 2016, pp. 770–778.
- [39] G. Huang, Z. Liu, L. Van Der Maaten, and K. Q. Weinberger, “Densely connected convolutional networks,” in *IEEE Conf. Comput. Vis. Pattern Recog.*, 2017, pp. 4700–4708.
- [40] C. R. A. Chaitanya, A. S. Kaplanyan, C. Schied, M. Salvi, A. Lefohn, D. Nowrouzezahrai, and T. Aila, “Interactive reconstruction of monte carlo image sequences using a recurrent denoising autoencoder,” *ACM Trans. Graph.*, vol. 36, no. 4, pp. 1–12, 2017.
- [41] Z. Cheng, H. Sun, M. Takeuchi, and J. Katto, “Performance comparison of convolutional autoencoders, generative adversarial networks and super-resolution for image compression,” in *IEEE Conf. Comput. Vis. Pattern Recog. Worksh.*, 2018, pp. 2613–2616.
- [42] X.-J. Mao, C. Shen, and Y.-B. Yang, “Image restoration using convolutional auto-encoders with symmetric skip connections,” *arXiv preprint arXiv:1606.08921*, 2016.



- [43] A. Krizhevsky, G. Hinton *et al.*, “Learning multiple layers of features from tiny images,” *Tech Report*, 2009.
- [44] W. Lin, “Visual perception and jnd modelling: progress and challenges,” *Workshop Keynote, Data-driven Just Noticeable Difference for Multimedia Communication, IEEE Int. Conf. Multimedia and Expo*, 2020.